A Two degrees of freedom system for wheel traction applications

Sara Roggia, *Member*, Francesco Cupertino, *Senior Member,*
Chris Gerada, *Member*, Michael Galea, *Member*

***Abstract*—In this paper, the use of conical induction machines is proposed for an in-wheel traction application. Such machines offer a rotational movement combined with a translational motion of the rotor. The horizontal movement is essential when active engagement and disengagement of the motor from the wheel without any extra mechanical component is required. This paper first investigates the basic concepts of how the conical machine functions and then proposes a mission strategy for a relevant traction application. A detailed description of the full scheme is given. In order to achieve the required performance, an innovative control method for both degrees of freedom of the machine (i.e. torque production and axial movement) is proposed and validated against a small-scale demonstrator of the whole system.**

***Index Terms*—conical motor, high voltage signal injection, in-wheel actuator, MEA, sensor-less control, axial force, sliding-rotor.**

I. INTRODUCTION

WITH the push towards the more electric aircraft (MEA) the aerospace community is focusing significant effort for the development of new electrical solutions for the enhancement of efficiency [1, 2], to reduce carbon footprint and to improve controllability and availability of aircraft. The general tendency is to move towards the introduction of electrical power production, electrical loads and new strategical managing solutions for reducing the energy consumed per flight [3-6]. With the advent of the MEA initiative [7-9], traditional systems are being replaced with more effective and reliable electrical counterparts [10],[11, 12].

View metadata, citation and similar papers at core.ac.uk
brought to you by CORE
provided by Nottingham eTheses

related to the operation of the aircraft on the ground, such as during the taxiing and push-back cycles. Recent initiatives in this area have focused on the implementation of a fully electrical system for maneuvering the aircraft on the ground [13-22] in order to avoid and/or reduce the use of the main engines or the traditional airport tow trucks. Such systems usually comprise the presence of a wheel actuator (WA) integrated into the landing gear (LG), in order to achieve aircraft traction on the ground. These technologies have shown various advantages such as for example up to 4 % of fuel saved per flight, improved on-time performances, and emission reductions, less airport noise, higher aircraft autonomy and lower tyre maintenance expenses.

The aforementioned benefits have been quantified through a different number of studies [23-25] and also confirmed with elaborate testing procedures [26, 27].

While several electrical taxiing systems exist today, a popular and common scheme is to include a gearbox and/or clutch system as connecting elements between the WA and the wheel [15, 17, 19, 21, 28]. In [29-32], a direct drive (DD) permanently connected WA has been chosen as the best option to meet the peak torque demand within the maximum accessible volume in the main LG. The DD WA consists of a high-performance permanent magnet (PM) machine with an outer rotor configuration. The PM motor is directly connected to the wheel without any reduction gearbox, which means that the speed of the motor is fixed by the speed of the wheel and vice-versa. Considering 1) the permanently-connected nature of the system, 2) the fact that the motor was designed for the relatively low-speed requirements of taxiing and 3) that the machine in question is a PM motor, then during the relatively high operating speeds of the take-off and landing phases, excessive levels of voltage are induced in the PM machine. In [31], it was discussed how the open terminal voltage (back-EMF) for that machine can exceed 4kV, which would result in irreversible damage to the motor.

In order to mitigate this risk, a feasible methodology of active engagement/disengagement between motor and wheel is e use of an active clutch or an integrated clutch [14, 15]. However, such solutions increase the component count (thus reduce reliability) and most importantly increase significantly the total system weight.

An innovative methodology for the required active engagement/disengagement capability with no extra cost to the system is thus proposed in this paper. The proposed solution is

Manuscript received April 19, 2017; revised July 16, 2017; accepted October 11, 2017. This work was partly supported by the "EU FP7 funding via the Clean Sky JTI – Systems for Green Operations ITD".

This work was also partly funded by the European Commission under the project titled INNOVATE, FP7 project number 608322 which is part of the FP7-PEOPLE-2013-ITN call and is hosted by the Institute for Aerospace Technology at the University of Nottingham.

Sara Roggia is with University of Nottingham and with Motor Design Limited, Wexham, UK (e-mail: Sara.Roggia@motor-design.com). Francesco Cupertino is with Politecnico di Bari, Bari, Italy (e-mail: cupertino@poliba.it). Chris Gerada and Michael Galea are with University of Nottingham, Nottingham, UK and with University of Nottingham Ningbo China (e-mails: chris.gerada@nottingham.ac.uk, michael.galea@nottingham.ac.uk).

that of using a conical motor system [33]. The inherent translational movement of the rotor within the conical machine is exploited to perform the disengagement of the motor from the wheel whilst the rotational movement is utilized to accomplish the aircraft traction.

In this work, a readily available, conical induction machine [34] is chosen to proof the concept and perform the traction and the engagement and disengagement operations. A purposely-built test-rig connected to a trolley wheel via an appropriate connection element is designed and developed.

The main challenge that surfaced during this work, was the appropriate control for the axial movement of the induction motor at hand. An innovative axial movement monitoring algorithm, proposed and validated in [35], was implemented onto the system. The results in terms of axial movement and position are therefore given in this paper. This 'sensor-less' technique represents an additional feature that can be implemented onto the system without any challenges in terms of extra space required, extra component count or being a single point of failure due to the harsh operating environment, since it does not make use of linear position or travel sensors.

II. Axial Force Generation in Conical Motors

A conical motor is an electrical machine in which the stator and the rotor do not follow the traditional concentric configuration of motors. For such machines, the conical shape is determined by the cone angle γ, calculated at the vertex of the cone, as shown in Fig. 1b.

A. The Concept

As for traditional machines, the total amount of force acting on the air gap element area can be divided into two main components, F_n and F_t, defined as the normal and the tangential forces with respect to the rotor lateral surface.

However, if a cylindrical reference frame is considered, then the normal component of the total magnetic force can be estimated as the sum of two contributions, namely the radial and the axial force, F_r and F_z.

For any electrical machine, apart from the torque-producing shear stress on the rotor surface, the radial forces are partly dependent on the inherent attraction between the stator and the rotor. For a magnetically balanced machine, these forces are usually negligible as the resulting vector sum of radial stresses over the rotor circumference approaches zero. Any remaining unbalanced pull is usually absorbed and held rigid by the machine bearings.

The main difference between a cylindrical and a conical machine is the presence of the axial force, F_z. It is well-known that the normal magnetic force is oriented perpendicularly to the lateral surface of the rotor. As shown in Fig. 1a, for conventional machines, the normal force coincides with the radial component and therefore does not have an axial contribution (i.e. parallel to the axial direction of the machine). Thus, the axial component of the total force is negligible when the rotor has a cylindrical shape.

However, for a conical configuration such as that of Fig. 1b, the normal force does have an axial component and, assuming that the right mechanical configuration is present (e.g. sliding bearings), the resulting total axial force can become significant and useful, in terms of producing axial or lateral movements of the rotor. This concept is mathematically formulated and explained in the following sub-section.

B. The Theory

The aim of this section is to provide a mathematical formulation for the axial force. In order to separate the axial component (F_z) from its radial and tangential components (F_r and F_t), the total force **F** acting in the air gap element area of the conical machine has been expressed in cylindrical coordinates.

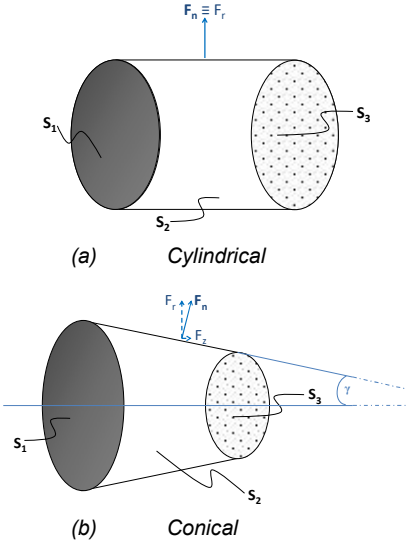

Fig. 1 - Generic air-gap forces

In Fig. 1a and Fig. 1b, the normal component (F_n) of the total force **F** is shown for both cylindrical and conical configurations. In both cases, the normal force F_n has the same direction of the vector normal to the lateral surface of the rotor, indicated as S_2. Within the cylindrical reference frame ($\overrightarrow{e_r}, \overrightarrow{e_\vartheta}, \overrightarrow{e_z}$), the vector normal to the cylindrical later surface of Fig. 1a has only the radial component (**n**=[1 0 0]). This confirms that the *z-axis* contribution of the normal force is null.

In Fig. 1b, the direction of the normal vector is perpendicular to the plane of conical rotor lateral surface S_2 defined by the cone angle γ. In this case, the components of the vector depend on the angle γ as demonstrated by the expression described by (1).

$$\mathbf{n} = \begin{bmatrix} \cos\gamma \\ 0 \\ \sin\gamma \end{bmatrix} \tag{1}$$

The total force acting on the conical rotor is the divergence of Maxwell's Stress Tensor *MST* ($\overleftrightarrow{T}$) on the cone volume (V), as described by (2). Considering the *divergence theorem* in vector calculus, the problem can be simplified as the integral of the force density, f, on the surface enclosing the conical body (area S_2) as given in (3), where **n** is the normal vector to the conical surface S_2 calculated in the same manner as shown in (1).

$$\mathbf{F} = \int_V \nabla \vec{T} dv \tag{2}$$

$$\mathbf{F} = \int_{S_2} f\mathbf{n} ds \tag{3}$$

As the *MST* represents a force density relative to a magnetic origin, the total force density, **f**, can be expressed using the normal and tangential components of the *MST*. As shown in [34], the normal σ and tangential τ magnetic stresses, derived by (4), depend on the normal and tangential components of the flux density (B_n and B_t). Therefore, the radial, tangential and axial components of the force density (respectively f_z, f_z, f_z) are obtained in (5) as functions of the flux density by combining the magnetic stresses expression of (4) and the formulation of the normal vector to the conical surface of (1).

$$\sigma = \frac{B_n^2 - B_t^2}{2\mu_0}; \quad \tau = \frac{B_n B_t}{\mu_0} \tag{4}$$

$$\mathbf{f} = \begin{bmatrix} f_r \\ f_t \\ f_z \end{bmatrix} = \frac{1}{2\mu_0} \begin{bmatrix} (B_n^2 - B_t^2)\cos\gamma \\ 2B_n B_t \\ (B_n^2 - B_t^2)\sin\gamma \end{bmatrix} \tag{5}$$

In order to quantify the axial component of the force, further simplifications are included by using the assumptions for law-saturated machines formulated in [35], where the tangential flux density can be neglected within the normal stress computation. In consideration of this simplification, the force density expression of (5) is rewritten as given in (6).

$$\mathbf{f} = \begin{bmatrix} f_r \\ f_t \\ f_z \end{bmatrix} = \frac{1}{2\mu_0} \begin{bmatrix} B_n^2 \cos\gamma \\ 2B_n B_t \\ B_n^2 \sin\gamma \end{bmatrix} \tag{6}$$

Implementing the estimation of the force density obtained in (6) within the total force calculation of (3), the following expression of the force is obtained:

$$\mathbf{F} = \begin{bmatrix} F_r \\ F_t \\ F_z \end{bmatrix} = \frac{\pi L_\gamma \bar{r}_g}{2\mu_0} \begin{bmatrix} B_n^2 \cos\gamma \\ 2B_n B_t \\ B_n^2 \sin\gamma \end{bmatrix}. \tag{7}$$

$$L_\gamma = \frac{L}{\cos\gamma}; \; \bar{r}_g = \frac{r_{s,\max} + r_{s,\min}}{2} \tag{8}$$

The third row of (7) represents the axial force exerted by the motor which is dependent on the level of flux density in the air gap. It is worth noting that in (7), it is the equivalent motor length (L_γ) and the medium air-gap radius ($\bar{r}_g$) that are adopted for the calculation of the force. These are calculated as in (8) on the consideration that L is the axial length of the motor and $r_{g,max}$ and $r_{g,min}$ represent the maximum and minimum air gap radius, respectively as shown in Fig. 2. These measurements enable to take in account the effect of the cone angle on the effective length of the machine and the fact that the radius in not constant over the all motor. The axial force is calculated at mid-point of the axial length of the motor considering the airgap flux density extracted around the medium radius of the machine. Since a minimum difference exists in the flux density distribution evaluated at different positions along the motor axial length, a valid estimation of the force can be obtained using the "medium" value of B_n and B_t in (7) extracted at at the central vertical cross section axis AA′ of Fig. 2.

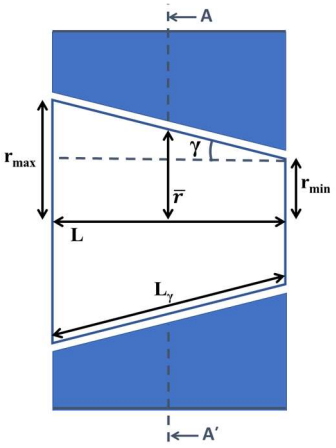

Fig. 2 - Conical Machine Cross-Section

In order to explicitly relate the axial force production to the amount of current that is required from the motor, the peak value flux density has been defined as a function of the motor features as described in (9), where p is the number of pole pairs, m is the number of phases, k_w is the winding factor, N number of turns and g' is the effective air gap length.

$$\hat{B} = \sqrt{2}\mu_0 \frac{mk_w NI}{\pi p g'} \tag{9}$$

If the motor is controlled with the d-axis field-producing current, then no tangential contribution to the total force exists, since the presence of the tangential stress depends on the q-axis torque-producing current. This means that the flux density will be mainly oriented to the normal axis and its value can be calculated as shown in (9). Therefore, the estimation of the axial force standing to the value of the motor current can be obtained implementing the expression of the flux density in the axial force calculation of (7). Specifically, if only the magnetizing current is produced using traditional vector control techniques [36], then the axial movement and the rotational movement of the rotor are not expected to occur at the same time. This enables the decoupling of the axial force production from the torque production of the machine. The use of the magnetizing current to obtain the axial movement of the rotor represents the central aspect of the implementation strategy illustrated in the next section.

III. TRACTION STRATEGY

As mentioned above, a conical induction machine has been selected for an electric traction application. The idea is to achieve active detachment of the actuator from the wheel without adding any external component. During take-off and landing, the motor should be fully disengaged from the aircraft wheel. In the context of this work, the chosen strategy is that the WA is "normally off", i.e. it engages only during its required

taxiing operation window. Thus, the 'normal', initial position of the system is represented by the rotor being fully retracted.

The flowchart of Fig. 3 gives a visual representation of the entire mission cycle procedure and includes the use of the axial monitoring algorithm to assess the rotor position. The awareness of the status of the system represents an essential aspect of the proposed configuration. It is indispensable to confirm that the motor is completely disengaged from the wheel before performing take-off or landing.

Before push-back from the gate with the turbo-fans still off, the first task is to engage the motor to the wheel. This is done through the proposed axial monitoring procedure (explained in the next section) that determines the rotor position by considering the magnetizing current and motor saliency. Based on the conclusions conveyed in the previous section, the *d*-axis current is utilized to produce the axial force required for axial rotor movement. The magnetizing current is increased until the engagement of the rotor is confirmed through the axial position monitoring system. As demonstrated in the experimental section, the complete attachment between the motor and the wheel happens when the current equals the rated value and the rotor reaches the full extended position. At this point, the system is then controlled in terms of torque production to push-back the aircraft from the gate and then taxi the aircraft to the main runway.

Once, the aircraft is on the runway and ready to take-off, then disengagement between motor and wheel is achieved by reducing the *d*-axis current. The axial position estimation algorithm helps in tracking the axial rotor position and establishes if the aircraft is ready to take-off. Simultaneously to this, the aircraft engines will be starting up, in preparation for take-off.

After landing, the whole procedure is repeated again in reverse, i.e. the motor is kept disengaged before and during landing. As soon as the aircraft is off the main runway, the engines can be switched off and the electrical taxiing system engaged.

As highlighted above, a critical point of all this is the ability to successfully engage the motor to the wheel via the proposed *d*-axis current control scheme and monitor it accurately through the rotor axial position algorithm assessment. The next section is therefore dedicated to the validation of these concepts, where the main aim is to demonstrate the importance of having a functioning and safe engaging/disengaging system.

IV. SCALED-DOWN DEMONSTRATOR

In order to demonstrate the feasibility of the proposed solution, the working principle of the conical actuator and the importance of having the axial position estimation monitoring, a scaled-down demonstrator has been built.

The complete system is shown in Fig. 4a, where the conical induction motor is connected to a small trailer wheel through a mechanical connection system. The mechanical engaging system consists of a small coupling with tapered teeth that are able to slide one on top of the other until the complete engagement is achieved, thus removing the need for accurate synchronization and positioning between the wheel and the motor. The mechanical coupling is illustrated in Fig. 4b.

Fig. 3 - Taxiing Strategy

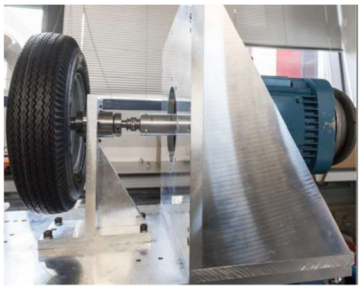

(a) Complete System

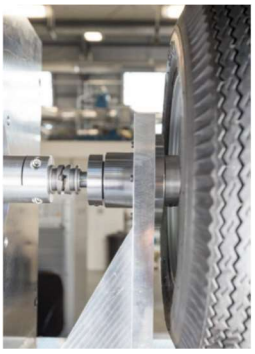

(b) Coupling System

Fig. 4 - Scaled-down Demonstrator

The control of the motor for the axial and rotational movement and the implementation of the axial monitoring scheme, as displayed in Fig. 7, have been realized in a Simulink® environment. The control system is implemented on a commercial dSpace 1103 platform. A set of duty cycles is generated by the control scheme and sent to a Texas Instruments TMS320F240 DSP running at 20 MHz which generates the signals used to drive the IGBT gates of a 750W inverter. IGBTs features are: 4 Arms rated current, 400 DC V rated voltage and 24 kHz switching frequency. A balanced system of three phase voltage signals is produced by the inverter and supplied into the motor. The real-time control and system monitoring is realized through a graphical user interface (GUI) opportunely customized. The power electronics' set-up is displayed in Fig. 5.

A. Motor Features and Control Scheme

The geometrical configuration of the conical machine is illustrated in Fig. 6, where an existing conical air gap between the stator and the rotor can be observed.

The forces on the conical air gap element produced by the interaction between rotor and stator cause the axial movement of the rotor that enables the engagement of the wheel. The machine has lap stator windings and aluminum squirrel-caged rotor. The main features of the motor are listed in Table I.

The 'normally off' position (i.e. rotor in the retracted position) is ensured with a spring that is located on the motor shaft in the front part of the case. The spring constant is equal to 6.67 N/mm^2. The maximum axial movement that the rotor can accomplish is equal to 4mm, depending on the accessible clearance within the stator case.

TABLE I - MOTOR FEATURES

Symbol	Quantity	Value
I	Rated Current	4.8 A
T	Rated Torque	14.3 Nm
rpm	Rated Speed	500 rpm
V	Rated Voltage – Wye Connection	400 V
p	Number of poles	12
f	Rated frequency	50 Hz
N	Number of turns per Phase	588
N_s	Number of Stator Slots	36
m	Number of phases	3
R_s	Stator Resistance	4.873Ω
σL_s	Stator Transient Inductance	107.343 mH
g	Mechanical Air-gap	1 mm
$r_{g,max}$	Max Stator bore radius	62.75 mm
$r_{g,min}$	Min Stator bore radius	42.5 mm
L_γ	Active Length	123 mm
γ	Cone Angle	9.35 Deg
I_m	Magnetizing Current	4.3 A
L_m	Magnetizing Inductance	170 mH
x	Maximum Axial Displacement	4 mm

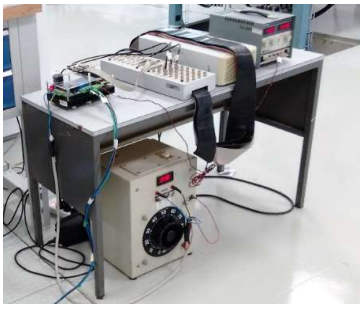

Fig. 5 - Motor Control Set-up

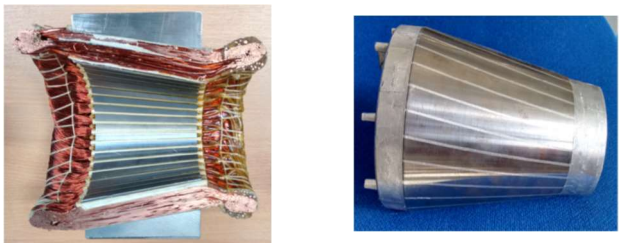

(a) Stator (b) Rotor

Fig. 6 - Cross-section of the Conical Induction Motor

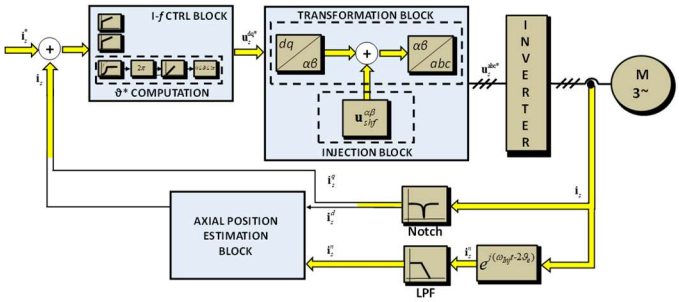

Fig. 7 - Control Scheme

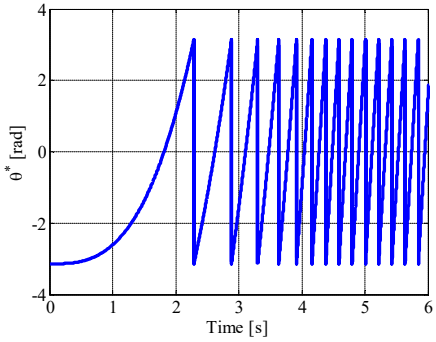

Fig. 8 - Control Angle

The control scheme implemented on the controller board has been reproduced in Fig. 7. The control strategy lies in the regulation of the magnetizing current (*d*-axis current) to perform the engagement and disengagement movement of the motor whereas the *q*-axis current is utilized in order to generate the rotational motion. The regulation of the current is realized through the use of common PI regulators.

The rotational movement is achieved through a sensorless scalar control strategy, known as I-*f* control [37-39]. This method utilizes constant *d*-axis and *q*-axis currents and an incremental frequency signal, calculated as in (10), where *k* is a positive constant.

$$f^* = kt^2 \tag{10}$$

From the frequency signal, the control angle (ϑ^*) is computed as described in (11) and displayed in the "ϑ Computation" block of Fig. 7. An output signal similar to Fig. 8 is generated by the "I-f Control Block".

$$\vartheta^* = \int 2\pi f^* dt \tag{11}$$

The I-f control strategy has been chosen in order to avoid the presence of rotational position transducer. A specific mechanical set-up is required to install a rotational speed transducer on this motor; the presence of the axial movement, in fact, can affect the normal functioning of the transducer if no alternative mounting measures are adopted. For the application at hand, this sensorless technique resulted more suitable than the traditional V/Hz control, as it offers the possibility to directly control the amplitude of the current vector. When the motor speed represents an essential requirement, the benefits of this sensorless control method can be combined with well-documented, speed estimation techniques [40] for determining the wheel speed without the use of rotational sensors. This contributes to an increase in the reliability of the whole system.

B. Axial Force Calculation

In order to quantify the axial force produced by the machine during the complete compression and decompression phases of the spring, measurements have been performed by locking the motor at a fixed axial position using an end-stop plate, similar to the one showed in Fig. 9.

Measurements are taken by using a load-cell attached to the plate. The required magnetizing current responsible for the axial force production has been obtained through the use of the current control loop implemented for the d-axis of the synchronous system. Since the rotor reaches the maximum extended position when the current equals the rated value, the axial force has been measured using current steps of 0.5A starting from zero up to the rated motor current. When the motor rated current is reached, in fact, the forced produced by the conical machine overcomes the spring force and the engagement happens. The decompression of the spring occurs when the current becomes lower than 2A.

At each level of the requested magnetizing current, the axial force exerted by the motor on the load-cell has been recorded. The experimental data has then been compared with analytical results achieved using the formulation of the axial force given in Section IIAs shown in Fig. 10, very good matching has been found between the analytical and experimental results, proving the validity of the axial force estimation method. The tests also confirmed that the proposed methodology of using the magnetization current only is inherently independent of the torque producing element (i.e. rotational torque). In fact, the axial movement can be controlled without instigation of any rotational movement in the system.

C. Axial Movement Assessment

The integration of the axial movement monitoring algorithm within the implementation scheme of the conical machine enables the horizontal movement of the rotor inside the stator to be monitored.

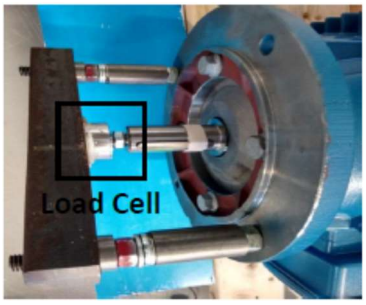

Fig. 9 - End-Plate with Load Cell

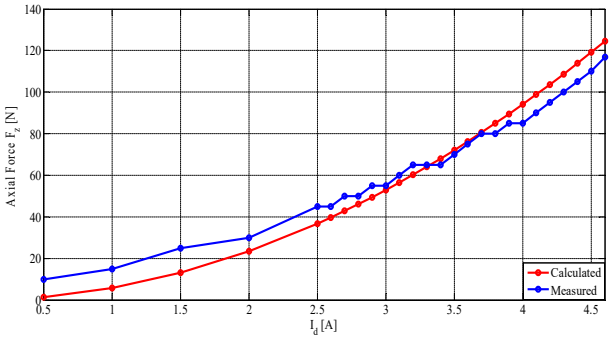

Fig. 10 - Analytical vs Experimental Axial Force

As mentioned above, this is dependent and proportional to the level of magnetizing current and the motor saliency. The monitoring procedure, in fact, is based on a self-sensing technique [41, 42] that requires the injection of a high-frequency voltage signal and then tracks changes in the machine parameters in order to relate them to the rotor axial position. A perceived advantage of this 'sensor-less' technique is, of course, the lack of dependency on linear position sensors, which could be detrimental in terms of component count and system reliability. This is also related to the harsh operating environment of the LG.

A high-frequency voltage of 120V-500Hz is superimposed on the supply voltage with 50Hz fundamental frequency. As displayed in the "Injection Block" of Fig. 7, the high-frequency voltage is generated and added to the main voltage in $\alpha\beta$ reference frame, thus it represents a rotating vector. As demonstrated in [41, 42], the changes in motor saliency cause the variation of the amplitude of the negative sequence signal of the high-frequency current response (I_n) to the injection signal. The values of I_n have been recorded for different levels of magnetizing current (I_d) and different axial positions. A 3D mapping of the axial rotor position has been completed based on the level of I_d and I_n as shown in Fig. 11. In order to optimize (in terms of computational resources) the axial monitoring procedure, the 3D look-up table (LUT) of Fig. 11 has been transformed into several 2D LUTs that relate the negative-sequence current to the axial position for a constant level of magnetizing current. The 2D LUTs have been implemented in the Axial Position Estimation Scheme of Fig. 13.

The realized algorithm chooses the appropriate axial position using the feedback signal of the magnetizing current and the negative-sequence current obtained through filtering and demodulation operations displayed in the homonymous block

Fig. 7.

The results of the monitoring system have been reported in order to demonstrate that the horizontal movement of the motor occurs whenever the force developed by the motor overcomes the spring load.

In Fig. 12, it can be observed that the axial movement of the rotor occurs when the magnetizing current reaches the nominal value. The transient phenomenon in the feedback *d*-axis current signal is due to the damping effect of the spring. When I_d is at the rated value, then the axial force developed by the motor is comparable to the one of the spring and thus as the motor force starts to slightly exceed the spring loading, then the rotor starts to move from its complete retracted position until it reaches its full extended position. The negative-sequence signal (I_n) increases in response to the voltage signal injection. The axial position estimation algorithm detects the variation in I_n signal and modifies its output relative to the instantaneous axial position. In Fig. 12, the feedback current and the axial position have been scaled by a factor of 100 for visualization purposes.

Therefore, all this demonstrates the validity of the proposed scheme. The axial position estimation depends on the level of the magnetizing current in the induction machine and when integrated into the full control scheme the *d*-axis current is then increased until the full extended axial position is registered and complete engagement is confirmed. On the contrary, to disengage the system, the magnetizing current will be reduced until the zero axial position is reached, such as to enable the landing and take-off aircraft procedures.

V. CONCLUSION

In this paper, the implementation of an elegant and simple engagement/disengagement system for an in-wheel traction application has been presented. As vessel to test the concept, an aircraft traction application was considered. With the proposed scheme, the need for a separate, active clutching system is removed. The scheme is based upon the utilization of conical machines, whose inherent shape and geometry permit both a rotational torque production and an axial, lateral movement. In this paper, the conical machine chosen to prove the concept was an induction machine, where the inherent machine aspects (such as the lack of permanent excitation) were taken advantage of to provide the required operation.

This was done by controlling the induction machine's magnetizing current in such a manner to allow an active connecting and disconnecting the motor from the wheel. It was shown how the axial force evaluation based on the *d*-axis manipulation proves that the axial movement of the rotor can be generated separately from the rotational motion.

The proposed traction concept and control strategy were validated against experimental results achieved on a purposely-built scaled-down demonstrator. The system has been arranged with a spring to hold the rotor in retracted position when the aircraft is not performing taxiing.

Due to the novelty of the proposed solution, no terms of comparison have been found for this specific system design. However, since the concept of the motor self-engagement/disengagement has been validly proven on the scaled-down model, further studies are already being undertaken by the authors in order to evaluate possible additional implications when the idea of the conical actuator is applied on a more realistic demonstrator.

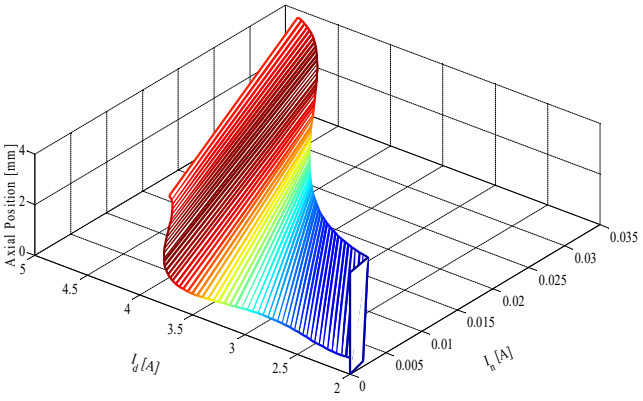

Fig. 11 - 3D Mapping of Axial Position

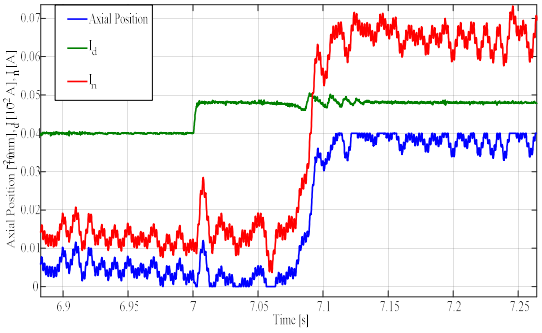

Fig. 12 - Axial Position estimation

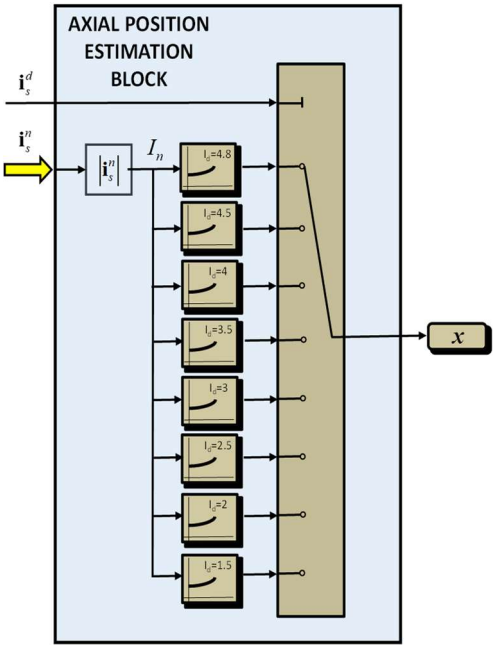

Fig. 13 - Axial Position Estimation Scheme

REFERENCES

[1] B. Sarlioglu and C. T. Morris, "More Electric Aircraft: Review, Challenges, and Opportunities for Commercial Transport Aircraft," *IEEE Transactions on Transportation Electrification,* vol. 1, pp. 54-64, 2015.

[2] R. I. Jones, "The More Electric Aircraft: the past and the future?," in *IEE Colloquium on Electrical Machines and Systems for the More Electric Aircraft (Ref. No. 1999/180)*, 1999, pp. 1/1-1/4.

[3] J. W. Bennett, G. J. Atkinson, B. C. Mecrow, and D. J. Atkinson, "Fault-Tolerant Design Considerations and Control Strategies for Aerospace Drives," *IEEE Transactions on Industrial Electronics,* vol. 59, pp. 2049-2058, 2012.

[4] M. Olaiya and N. Buchan, "High power variable frequency generator for large civil aircraft," in *IEE Colloquium on Electrical Machines and Systems for the More Electric Aircraft (Ref. No. 1999/180)*, 1999, pp. 3/1-3/4.

[5] A. J. Mitcham and J. J. A. Cullen, "Permanent magnet generator options for the More Electric Aircraft," in *2002 International Conference on Power Electronics, Machines and Drives (Conf. Publ. No. 487)*, 2002, pp. 241-245.

[6] L. d. Lillo, L. Empringham, P. W. Wheeler, S. Khwan-On, C. Gerada, M. N. Othman*, et al.*, "Multiphase Power Converter Drive for Fault-Tolerant Machine Development in Aerospace Applications," *IEEE Transactions on Industrial Electronics,* vol. 57, pp. 575-583, 2010.

[7] "IEE Colloquium Electrical Machines and Systems for the More Electric Aircraft," in *IEE Colloquium on Electrical Machines and Systems for the More Electric Aircraft (Ref. No. 1999/180)*, 1999, pp. 0_7-0_8.

[8] P. Wheeler and S. Bozhko, "The More Electric Aircraft: Technology and challenges," *IEEE Electrification Magazine,* vol. 2, pp. 6-12, 2014.

[9] A. Tenconi and P. W. Wheeler, "Introduction to the Special Section on The More Electric Aircraft: Power Electronics, Machines, and Drives," *IEEE Transactions on Industrial Electronics,* vol. 59, pp. 3521-3522, 2012.

[10] C. Gerada and K. J. Bradley, "Integrated PM Machine Design for an Aircraft EMA," *IEEE Transactions on Industrial Electronics,* vol. 55, pp. 3300-3306, 2008.

[11] M. Galea, C. Gerada, T. Raminosoa, and P. Wheeler, "A Thermal Improvement Technique for the Phase Windings of Electrical Machines," *IEEE Transactions on Industry Applications,* vol. 48, pp. 79-87, 2012.

[12] C. I. Hill, S. Bozhko, Y. Tao, P. Giangrande, and C. Gerada, "More Electric Aircraft Electro-Mechanical Actuator Regenerated Power Management," in *2015 IEEE 24th International Symposium on Industrial Electronics (ISIE)*, 2015, pp. 337-342.

[13] R. W. Jenny, "Aircraft wheel drive apparatus and method," ed: Google Patents, 1976.

[14] I. W. Cox, H. J. Walitzki, and J. S. Edelson, "Motor for driving aircraft, located adjacent to undercarriage wheel," ed: Google Patents, 2012.

[15] D. J. Christensen, T. Langston, D. L. Charles, and R. Velasquez, "Aircraft electric taxi system with friction actuated, bi-directional clutch," ed: Google Patents, 2013.

[16] N. Gilleran, R. M. Sweet, J. S. Edelson, R. T. Cox, and I. W. Cox, "Electric Motor Integrated with a Wheel," ed: Google Patents, 2012.

[17] J. Edelson and I. Cox, "Geared wheel motor design," ed: Google Patents, 2007.

[18] S. Sullivan, "Landing gear method and apparatus for braking and maneuvering," ed: Google Patents, 2007.

[19] R. M. Sweet and J. S. Edelson, "Motor and gearing system for aircraft wheel," ed: Google Patents, 2013.

[20] N. Gilleran, R. Sweet, and S. Perkins, "Split circumference aircraft wheel assembly with integrated drive motor assembly," ed: Google Patents, 2013.

[21] M. Schier, F. Rinderknecht, A. Brinner, and H. Hellstern, "High integrated Electric Machine for Aircraft Autonomous Taxiing," in *International Conference on Electric Vehicles and Renewable Energies EVER*, 2011, p. 31.

[22] T. F. Johnson, "Electric Green Taxiing System (EGTS) for Aircraft," in *IEEE Transactions on Transportation Electrification Web Portal*, ed, 2016.

[23] F. Re, "Assessing Environmental Benefits of Electric Aircraft Taxiing through Object-Oriented Simulation," *SAE Int. J. Aerosp.,* vol. 5, pp. 503-512, 2012.

[24] F. Re, "Viability and state of the art of environmentally friendly aircraft taxiing systems," in *2012 Electrical Systems for Aircraft, Railway and Ship Propulsion*, 2012, pp. 1-6.

[25] F. Re. An Object-oriented Model for Development and Assessment of Green Taxiing Systems [Online]. Available: http://elib.dlr.de/89055/

[26] WheelTug. (2016). *Aircraft Efficiency: New WheelTug System Saves About 7 Minutes Every Flight Departure (April 04, 2016 ed.)*. Available: http://www.marketwired.com/press-release/aircraft-efficiency-new-wheeltug-system-saves-about-7-minutes-every-flight-departure-2111601.htm

[27] M. Monaghan. (2014). *Airbus exploring electric taxiing solution for A320 Family* Available: http://articles.sae.org/12708/

[28] M. S. Hellstern, R. Frank, and Heribert, "Electric Wheel Hub Motor for Aircraft Application," *1,* 2012-01-14 2012.

[29] M. Galea, S. Roggia, L. Papini, Z. Xu, C. Tighe, M. Hamiti*, et al.*, "Design aspects of a high torque density machine for an aerospace traction application," in *Electrical Machines and Systems (ICEMS), 2014 17th International Conference on*, 2014, pp. 2773-2778.

[30] T. Raminosoa, T. Hamiti, M. Galea, and C. Gerada, "Feasibility and electromagnetic design of direct drive wheel actuator for green taxiing," in *2011 IEEE Energy Conversion Congress and Exposition*, 2011, pp. 2798-2804.

[31] M. Galea, "High Performance, Direct Drive Machines for Aerospace Applications," Doctor of Philosophy, Electrical and Electronic Engineering, The University of Nottingham, 2013.

[32] Z. Xu, M. Galea, C. Tighe, T. Hamiti, C. Gerada, and S. J. Pickering, "Mechanical and thermal management design of a motor for an aircraft wheel actuator," in *2014 17th International Conference on Electrical Machines and Systems (ICEMS)*, 2014, pp. 3268-3273.

[33] H. Bitsch and H. Mall, "Sliding rotor motor," ed: Google Patents, 1992.

[34] Z. Q. Zhu, M. L. M. Jamil, and L. J. Wu, "Influence of Slot and Pole Number Combinations on Unbalanced Magnetic Force in PM Machines With Diametrically Asymmetric Windings," *IEEE Transactions on Industry Applications,* vol. 49, pp. 19-30, 2013.

[35] G. Munteanu, A. Binder, and S. Dewenter, "Five-axis magnetic suspension with two conical air gap bearingless PM synchronous half-motors," in *Power Electronics, Electrical Drives, Automation and Motion (SPEEDAM), 2012 International Symposium on*, 2012, pp. 1246-1251.

[36] D. W. Novotny and T. A. Lipo, *Vector Control and Dynamics of AC Drives*: Clarendon Press, 1996.

[37] I. Boldea, A. Moldovan, and L. Tutelea, "Scalar V/f and I-f control of AC motor drives: An overview," in *2015 Intl Aegean Conference on Electrical Machines & Power Electronics (ACEMP), 2015 Intl Conference on Optimization of Electrical & Electronic Equipment (OPTIM) & 2015 Intl Symposium on Advanced Electromechanical Motion Systems (ELECTROMOTION)*, 2015, pp. 8-17.

[38] S. C. Agarli, x, x, F. M, x, tu*, et al.*, "I-f starting and active flux based sensorless vector control of reluctance synchronous motors, with experiments," in *Optimization of Electrical and Electronic Equipment (OPTIM), 2010 12th International Conference on*, 2010, pp. 337-342.

[39] M. Fatu, R. Teodorescu, I. Boldea, G. D. Andreescu, and F. Blaabjerg, "I-F starting method with smooth transition to EMF based motion-sensorless vector control of PM synchronous motor/generator," in *2008 IEEE Power Electronics Specialists Conference*, 2008, pp. 1481-1487.

[40] F. Briz, M. W. Degner, P. Garcia, and R. D. Lorenz, "Comparison of saliency-based sensorless control techniques for AC machines," *IEEE Transactions on Industry Applications,* vol. 40, pp. 1107-1115, 2004.

[41] S. Roggia, F. Cupertino, M. Galea, and C. Gerada, "Axial Position Estimation of Conical Shaped Motor for Electric Taxiing Application," presented at the IEEE Energy Conversion Congress and Expo (ECCE), Milwaukee, WI, 2016.

[42] S. Roggia, F. Cupertino, C. Gerada, and M. Galea, "Axial Position Estimation of Conical Shaped Motors for Aerospace Traction

Applications," *IEEE Transactions on Industry Applications,* vol. PP, pp. 1-1, 2017.

Sara Roggia (M'17) completed her Bachelor degree and her Master of Science degree in Electrical Engineering at the Politecnico di Bari, Italy. She is currently reading for a PhD in electrical machines design at the University of Nottingham, UK, as a Marie Curie Fellow. She has worked extensively on the development of novel electrical machines technologies for aircraft ground operations within the context of the more electric aircraft initiative. Since May 2017, Sara is a senior design engineer with Motor Design Limited (MDL) working on the design of different topologies of electrical machines and supporting the team for the software development. Her main areas of interests are the electromagnetic design and thermal management of electrical machines and more electric aircraft technologies.

Francesco Cupertino (M'08, SM'12), received the Laurea degree and the PhD degree in Electrical Engineering from Politecnico di Bari, Bari, Italy, in 1997 and 2001 respectively. Since 2001, he has been with the department of Electrical and Information Engineering of the Politecnico di Bari, where he is currently a full professor in converters, electrical machines and drives. His research interests include the design of synchronous electrical machines, motion control of high performances electrical machines, applications of computational intelligence to control, and sensorless control of ac electric drives. He is the author or co-author of more than 100 scientific papers on these topics. Since 2010, he has been the scientific director of the laboratory Energy Factory Bari (EFB), a joint initiative of the Politecnico di Bari and GE AVIO, aimed at developing research projects in the fields of aerospace and energy.In 2015 he received two best paper awards from the Electrical Machines Committee of the IEEE Industry Application Society and from the homonymous Committee of the IEEE Industrial Electronics Society.

Chris Gerada (M'05) received the Ph.D. degree in numerical modeling of electrical machines from The University of Nottingham, Nottingham, U.K., in 2005. He subsequently worked as a Researcher with The University of Nottingham on high-performance electrical drives and on the design and modeling of electromagnetic actuators for aerospace applications. Since 2006, he has been the Project Manager of the GE Aviation Strategic Partnership. In 2008, he was appointed as a Lecturer in electrical machines; in 2011, as an Associate Professor; and in 2013, as a Professor at The University of Nottingham. His main research interests include the design and modeling of high-performance electric drives and machines. Prof. Gerada serves as an Associate Editor for the IEEE TRANSACTIONS ON INDUSTRY APPLICATIONS and is the Chair of the IEEE IES Electrical Machines Committee.

Michael Galea (M'13) received his PhD in electrical machines design from the University of Nottingham, UK, where he has also worked as a Research Fellow and as an academic and as the Deputy Director of the University's Institute for Aerospace Technology in the UK. In 2017, he was appointed as the Head of the School of Aerospace in the University of Nottingham Ningbo China. He is also the Director of the Institute for Aerospace Technology at the University of Nottingham Ningbo China. He manages a number of diverse projects and programs related to the more / all electric aircraft, electrified propulsion and associated fields. His main research interests are the design, analysis and thermal management of electrical machines and drives and the more / all electric aircraft.